communications chemistry

Article

https://doi.org/10.1038/s42004-024-01362-5

Unlocking the potential of azide-phosphine Staudinger reaction for the synthesis of poly(arylene iminophosphorane)s and materials therefrom

Tomaž Kotnik[1,2], Antoine Debuigne[3], Julien De Winter[4], Matej Huš[1,5,6], Albin Pintar[1] & Sebastijan Kovačič[1,7]

Iminophosphoranes with the general formula ($R_3P{=}NR'$) have great potential in synthetic chemistry as valuable precursors/intermediates in organic synthesis or as building blocks for various organic compounds. However, the synthetic approaches and conditions to prepare iminophosphoranes are still poorly understood, limiting the utility of this chemistry for organic materials. In this article, a simple and efficient synthesis of previously unattainable poly(arylene iminophosphoranes) is reported. The azide-phosphine Staudinger polycondensation is used, and the reaction conditions are carefully studied, including consideration of light and air, the influence of solvent and temperature, and investigation of the electronic and steric effects of multiazides. The newly defined reaction conditions appear to be highly versatile, allowing the use of both electron-rich and electron-deficient arylazides for reaction with phosphines to synthesize a library of poly(arylene iminophosphorane) networks that exhibit exceptional thermal and oxidative stability. Interestingly, despite the ylidic-form of the iminophosphorane linkage as shown by theoretical calculations, these newly developed poly(arylene-iminophosphorane) networks exhibit semiconducting properties, such as absorption band edges up to 800 nm and optical band gaps in the range of 1.70 to 2.40 eV. Finally, we demonstrate the broad applicability of these polymers by processing them into glassy films, creating foam-like structures and synthesizing metallo-polymer hybrids.

Organic semiconductors are a broad class of carbon-based materials ranging from molecular crystals to amorphous molecular films and conjugated polymers (CP) with semiconductor properties. Especially CPs have gained popularity, as they are lightweight and mechanically flexible "plastic", which significantly increases their usefulness compared to inorganic analogs. The main advantage over inorganic analogs lies in the infinite combination possibilities of different structural motifs and, thus, functionalities within the polymer network at the expense of the extensive organic reaction toolbox. This opens up the opportunity for molecular customization, i.e. designing the properties of CPs at the molecular level and tailoring them to their specific needs.

It is a challenge to synthesize structurally ideal CPs, and defects in their structures can significantly impair their electronic functions. CP is usually synthesized by cross-coupling reactions that depend on transition-metal

[1]National Institute of Chemistry, Hajdrihova 19, SI-1001 Ljubljana, Slovenia. [2]Faculty of Chemistry and Chemical Technology, University of Ljubljana, Večna pot 113, SI-1000 Ljubljana, Slovenia. [3]Chemistry Department, Center for Education and Research on Macromolecules (CERM), CESAM Research Unit, University of Liege (ULiege), Quartier Agora, 13 Allée du Six Août (Bldg B6a), Sart-Tilman, B-4000 Liège, Belgium. [4]Organic Synthesis and Mass Spectrometry Laboratory (S2MOs), University of Mons-UMONS, Mons, 7000, Belgium. [5]Association for Technical Culture of Slovenia (ZOTKS), Založka 65, SI-1000 Ljubljana, Slovenia. [6]Institute for the Protection of Cultural Heritage of Slovenia (ZVKDS), Poljanska 40, SI-1000 Ljubljana, Slovenia. [7]Catalysis and Organic Synthesis Research Group, Faculty of Chemistry and Chemical Engineering, University of Maribor, Smetanova 17, SI-2000 Maribor, Slovenia. e-mail: sebastijan.kovacic@um.si

(TM) catalysis mechanisms[1]. Although these reactions produce intriguing π-conjugated macromolecular networks with well-defined molecular weights, defined chain-ends, and low dispersity (*Đ*), the TM-catalyst becomes a residual impurity in the polymer network and thus a potential "defect" that can impair the electronic functions of the CP[2,3]. Recently, alternatives such as photochemical methods[4,5], multicomponent polymerizations[6], or condensation-based reactions[7] have emerged as TM-free alternatives[8].

Of particular interest, are reactions in which no bis-organometallic (M; Sn, Mg, Cu, B) and/or bis-halide monomers (X; Br, I) are used in the synthesis and proceed without TM-catalysis. It has been demonstrated that the presence of C–X(M) end-groups in the π-conjugated polymer network resulting from these monomers can have a significant impact on the optoelectronic properties of CPs, similar to the effects of residual TM impurities[9,10]. Recently, organic reactions without TM-catalysts and organometallic- or halide-terminated monomers have become an important synthetic approach to obtain CPs, as they are simple, efficient and tolerant to functional groups compared to conventional cross-coupling reactions[7]. Examples are the Schiff base or Aza-Wittig reaction for the preparation of azomethine-linked CPs[11–13], the Knoevenagel reaction for cyanovinylene-linked CPs[14,15], the Aldol or Wittig reaction for the introduction of vinylene linkages[16–18] and the Horner–Wadsworth–Emmons reaction for trans-vinylene linked CPs[19,20], or the phospha-Wittig and Becker reaction for the phosphaalkene-linked CPs[21–23], to name a few. The linkages mentioned can significantly influence the electronic properties of CPs due to the different electronic structures of the heteroatoms in them. Phosphorus in phosphaalkenes, for example, is known to be a carbon-like element and extends conjugation, while nitrogen in the form of an azine-linkage represents a conjugation node and shortens effective conjugation.

In pursuit of the benefits of transition metal-free and halide-free chemistry, we examined a decades-old Staudinger reaction to explore its potential for the preparation of iminophosphorane-linked polymers, namely poly(arylene iminophosphorane; PAIP)[24]. PAIPs belong to the poly(organophosphazene) family. Poly(organophosphazene)s, a special class of molecular hybrid polymers, featuring both an inorganic (phosphorus–nitrogen) backbone and two organic substituents on each phosphorus atom (P)[25,26], making the P-centers pentavalent (λ^5) and tetracoordinated (σ^4) and thus robust[27]. Such unique hybridization imparts remarkable properties, including high thermal stability and inherent flame-retardant characteristics[27]. Poly(organophosphazene)s are usually synthesized through a ring-opening polymerization of hexachlorocyclotriphosphazene followed by macromolecular substitution reactions. However, this seminal synthesis method of Allcock et al., still in use today, comes with several drawbacks, including low hydrolytic stability of both precursors and products, the necessity for high temperatures (around 250 °C), and high vacuum conditions, among others[28].

The Staudinger reaction is an alternative synthesis approach for poly(organophosphazenes), especially for PAIPs. In the first step of this reaction, the nucleophilic phosphine moiety (i) attacks the azide (ii) to form the phosphazide intermediate, which undergoes intramolecular cyclization (iii) and leads to the formation of iminophosphoranes (iv), of the general formula (–R_3P=N–), with loss of gaseous nitrogen (Scheme 1A)[24]. However, only three reports are known in which the Staudinger reaction was used to synthesize PAIPs (Scheme 1B)[29–31]. In all previous attempts, relatively harsh synthesis conditions were used, and a considerable amount of phosphine (v) was oxidized to the phosphine oxide moiety (vii) (Scheme 1B). The oxidation process abates the nucleophilicity of the phosphorus in the (v) to react with (vi) and thus impairs the reaction rate to and yields of (vii) (Scheme 1B). Consequently, the Staudinger reaction was mostly restricted to reactive aryl azides, especially those that are electron-deficient, which limited the scope of PAIP synthesis as electron-rich aryl azides were not utilized.

In this work, we examine the azide-phosphine Staudinger reaction and redefine the synthesis conditions, including the determination of light and air effects, the study of electronic and steric effects of multiazides, and the influence of the solvent (Scheme 1C). We followed a bottom-up approach, starting with the Chan–Lam coupling reaction, and prepared a series of organic multiazide monomers (Fig. S1). The optimized synthesis conditions proved advantageous, leading to the successful synthesis of several previously unobtainable poly(arylene iminophosphorane)s, exhibiting structural motifs such as phenylene, 2,1,3-benzothiadiazole, 1,3,5-tris(phenyl) benzene, and 9,9-dioctylfluorene, with polymerization yields up to 99% and average weight molar mass up to over 12,000 g mol^{-1}, and dispersity (*Đ*) of 1.1−1.5. The optoelectronic properties, the bandgap structures, and the exceptional thermal and oxidative stability are discussed in detail and supported by calculations using time-dependent density functional theory (TD-DFT). Finally, the potential and versatility of our approach are vividly demonstrated by the successful preparation of the first poly(arylene iminophosphorane)-based glassy films, foams, and even metallo-polymers.

Results and discussion

Poly(arylene iminophosphorane) (PAIP) synthesis via the Staudinger polycondensation

A series of PAIPs were prepared by the Staudinger reaction of organic multiazides (**2a–e**, Fig. S1) with bis(diphenylphosphino)benzene (**3a**) or bis(diphenylphosphino)ferrocene (**3b**). The multiazide monomers were first synthesized in high yields (up to 98%) by a Chan–Lam cross-coupling of arylboronic acid pinacol ester derivatives and sodium azide (Fig. S1). To comprehensively investigate the azide-phosphine Staudinger reaction as a

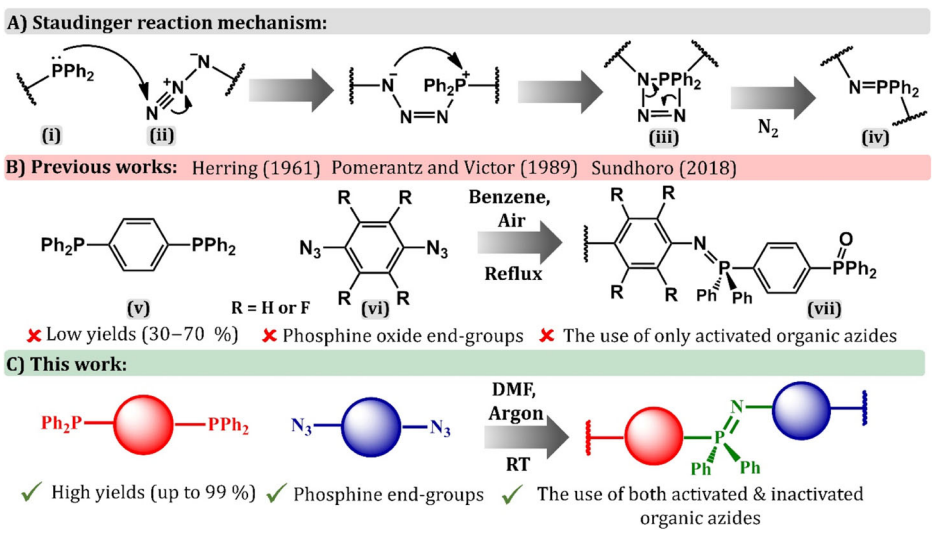

Scheme 1 | Background of Staudinger reaction. Reaction mechanism of the Staudinger reaction (**A**), current state of the art (**B**), and contributions of this work (**C**).

Table 1 | Optimization of reaction conditions for 4ca synthesis

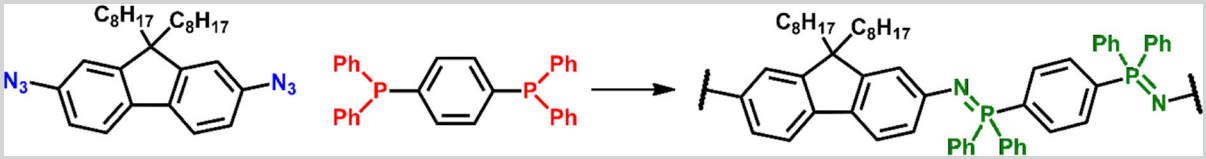

Entry	Solvent	Atmosphere	Temp (°C)	Conv (%)	Yield (%)	M_n (g/mol)	M_w (g/mol)	$Đ$
1	Toluene	Air	r.t.	96	71	3450	4650	1.34
2	DMF	Air	r.t.	97	78	3700	4380	1.18
3	Toluene	Argon	r.t.	99	91	5050	6640	1.32
4	DMF	Argon	r.t.	99	92	9100	12,900	1.41
5	Toluene	Argon	60	99	91	4730	6020	1.27
6	DMF	Argon	60	99	92	5480	8600	1.57

Conversions were determined using ^{1}H NMR spectroscopy, while yields were measured gravimetrically. Molecular weight characteristics were assessed by SEC in THF at 40 °C using a Viscotek 305 TDA chromatograph equipped with two columns (PSS SDV linear M 5 µm) and a triple detector (refractive index, viscometer, low angle light scattering) calibrated with a Malvern PS standard of 99 kDa.

polymerization chemistry, we chose 9,9-dioctyl-2,7-diazidofluorene (**2c**) and bis(diphenylphosphino)benzene (**3a**) as archetypal substrates (Table 1), since **2c** contains a soluble dioctylfluorene core that facilitated characterization. A series of important experimental parameters were investigated such as solvent choice (DMF or toluene), synthesis atmosphere (argon or air), and temperature (RT or 60 °C). Table 1 summarizes conversions and characteristics of the resulting polymers (**4ca**) measured by SEC with triple detection (refractive index, viscometer, low angle light scattering), such as weight average molar mass (M_w), number average molar mass (M_n) and dispersity ($Đ$). Initial reactions were carried out with equimolar amounts of **2c** and **3a** in air at room temperature. The product, **4ca**, was obtained in good yields (>71%) with near complete disappearance of the reagents (conversions > 96%) (Table 1, entries 1 and 2, respectively) and was characterized with ^{13}C and ^{31}P CP/MAS NMR (SI). The SEC analysis of **4ca** revealed modest molecular weights around 4500 g mol^{-1} in both DMF (entry 2) and toluene (entry 1) using solvent elution. This is in line with literature reports where Staudinger ligation proceeds rapidly in polar solvents due to the stabilization of the polar transition state[32]. The formation of the iminophosphorane linkage in **4ca** was confirmed in the ^{31}P CP/MAS NMR spectrum by the characteristic phosphorus peak at −2.3 ppm (Table 1 and Fig. 1A). The deconvolution of the rather broad peak revealed two contributions, the downshifted peak for the phosphazene linkage at about −2 ppm, and the upshifted peak for the phosphine end-groups at about −4 ppm (Fig. 1A). In addition, we observed a distinct peak at 29 ppm that can be assigned to the phosphine-oxide (–ArPh_2P=O) in the structure (Fig. S2)[33]. The formation of –ArPh_2P=O must have taken place during polymerization (vide infra), as it was not initially detected in the **3a**. Although aryl-iminophosphoranes (–[Ph_2P=NAr]$_n$–) are generally stable under humid conditions and tend to hydrolyze in the presence of dilute acids or bases[26,34], several control experiments were performed to check for possible hydrolysis or oxidation of the [Ph_3P=NAr]– end-groups in the PAIP. To analyze the extent of hydrolysis, **4ca** was synthesized under a moisture-free atmosphere (see SI) to avoid water attack on the –[Ph_2P=NAr]$_n$– linkages. However, ^{31}P NMR analysis revealed about 17% of the R_3P=O groups (Fig. S2), which was only slightly less than in the presence of water (i.e. 25%). In addition, FTIR analysis (Fig. S3) did not detect any amine groups that should be present after hydrolysis of the –[Ph_2P=NAr]$_n$– linkages, so it was concluded that the extent of hydrolysis was negligible. The next control was an inert atmosphere to analyze the extent of oxidation. Thus, the synthesis of **4ca** was carried out in an argon atmosphere and in dry conditions. In this case, the **4ca** was fully characterized by combining FTIR and ^{31}P CP/MAS NMR spectroscopy with the size exclusion chromatography (SEC) and matrix-assisted laser desorption/ionization time-of-flight (MALDI-ToF-MS) analysis (see SI). Under these conditions, better conversions (>99%) and yields (>92%) were achieved (Table 1, entries 3 and 4). Characterization by FTIR and ^{31}P CP/MAS NMR revealed the complete disappearance of the precursors' functional groups, i.e. phosphine (Fig. 1A) and azide (Fig. 1B), and the appearance of an iminophosphorane linkage in product **4ca**. In addition, the ^{31}P CP/MAS NMR analysis revealed a much lower peak corresponding to the –ArPh_2P=O groups (Fig. S4).

SEC analysis confirmed that **4ca** was produced with significantly higher molecular weights, reaching up to 12,900 g mol^{-1} in DMF (Table 1, entry 4). However, it is noteworthy that the SEC chromatograms revealed a multimodal profile (Fig. S5), and consequently, M_n and $Đ$ should be taken with care. The distinct sharp peaks on the higher elution time certainly correspond to oligomers resulting from side reactions limiting the degree of polymerization whereas the broader peak on the lower elution volume accounts for polymer chains with higher degrees of polymerization. As an indication, a dispersity of 1.4 was measured, but it should be taken with caution given the multimodal nature of the SEC peak. To gain insight into the possible side reaction and polymer defects, MALDI-ToF-MS analysis was performed (Figs. S6 and S7). The MS spectrum revealed different populations with peaks separated by an interval of 863 mass units (u), which corresponds to the mass of the **4ca** repeating unit (Fig. 1C). As expected for polymers with moderate-to-high $Đ$ and a M_w above 5000 g mol^{-1}, the intensity of the signals tends to decrease with increasing degree of polymerization, but the signals were still detectable up to m/z 10,000. However, it should be noted that the molar mass of polymers with a dispersity >1.2 cannot be directly deduced from the MALDI MS spectrum[35]. In fact, low molecular weight oligomers are significantly overestimated due to their easier desorption/ionization and detection efficiency. Figure S7 shows some possible populations that contain the phosphine function, the azide function, or one of both as polymer chain-ends. Finally, cyclic poly(arylene iminophosphorane) derivatives of low and moderate molecular weight are also detected, which certainly contribute to limiting the molar mass of the polymer (Fig. S7A). The Staudinger reaction was also carried out at 60 °C under inert and dry conditions, but no improvement in molecular weight was achieved (Table 1, entries 5 and 6). These controls show that oxidation is detrimental to Ph_2P–Ar–, which has a strong effect on the Staudinger reaction.

To clarify the oxidation mechanism of phosphine, we performed several photocatalytic experiments in which equimolar solutions of **2c** and **3a** in DMF were reacted under different conditions (Fig. 2A). The formation of –ArPh_2P=O end-groups was monitored by ^{31}P NMR analysis, where the amount of –ArPh_2P=O relative to the –[Ph_2P=NAr]$_n$– linkages in the PAIP

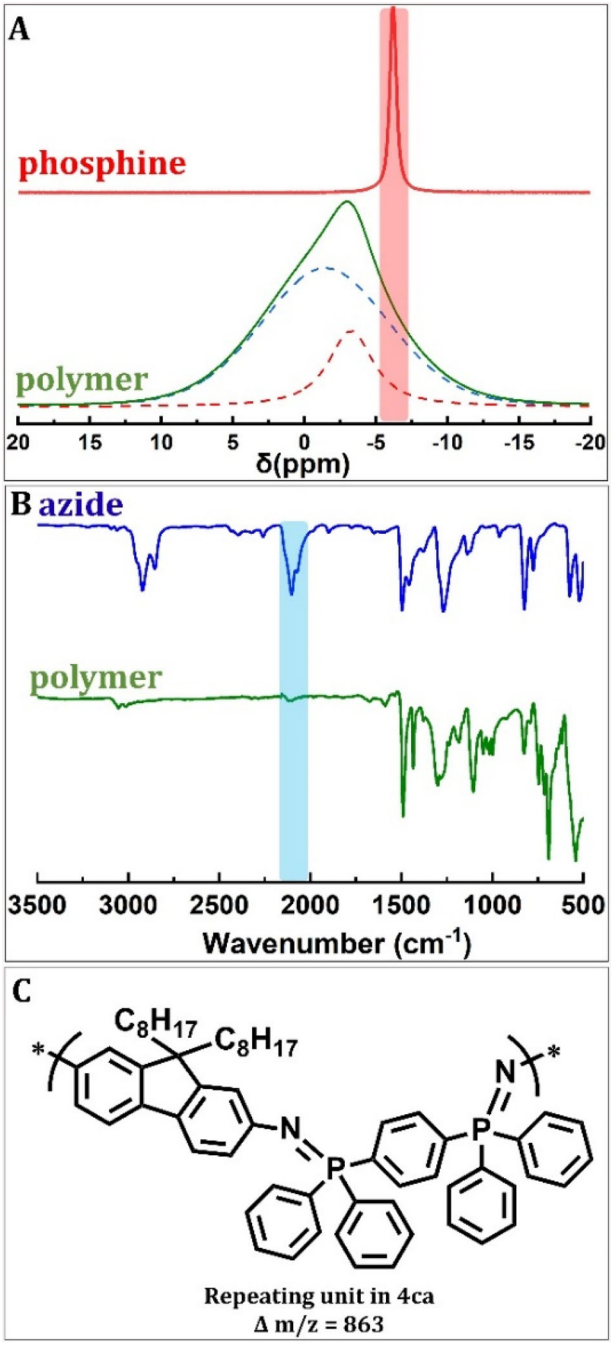

Fig. 1 | Conversion of monomers and repeating unit of model polymer 4ca. ^{31}P CP/MAS NMR (for the phosphine monomer **3a**) (**A**) used to follow the conversion to **4ca**; FTIR (for the azide monomer; **2c**) (**B**) and the repeating unit in **4ca** defined by MALDI-ToF-MS analysis (**C**).

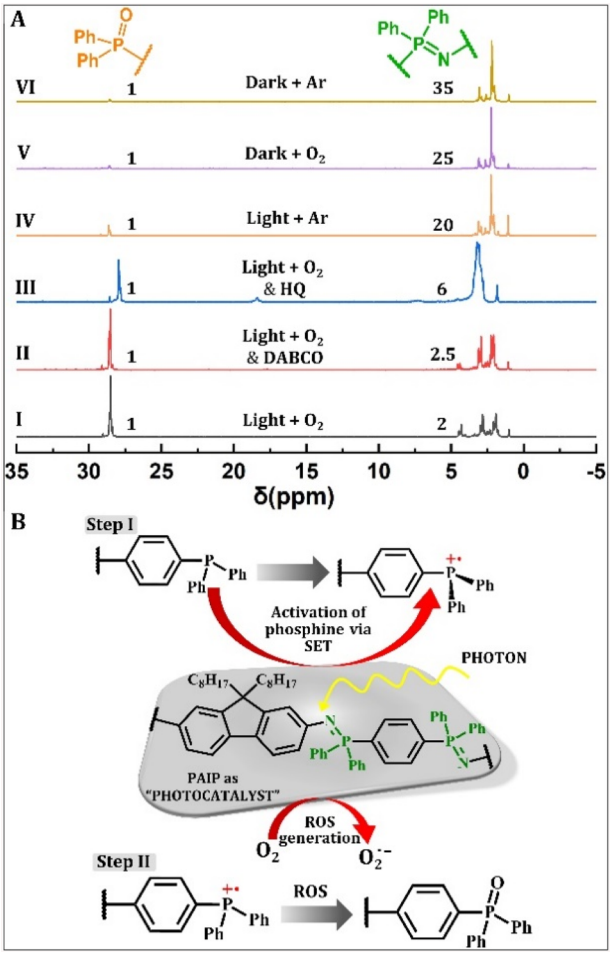

Fig. 2 | Influence of light and oxygen on the presence of phosphine oxide moiety. Quantitative ^{31}P NMR experiments for the investigation of light and oxygen effect on phosphine oxidation (**A**), and proposed mechanism of phosphine end-group oxidation (**B**) based on experiments and literature reports[36–38].

backbone was determined by peak integration (SI). The initial reaction was carried out under ambient conditions (visible light/air) and NMR analysis revealed the formation of oxidized phosphine end-groups in large amounts (–$ArPh_2P$=O/P=N integral ratio of 1:2; Spectrum I in Fig. 2A). Repeating this reaction in the absence of visible light and of atmospheric oxygen (dark/argon conditions), however, markedly improved the –$ArPh_2P$=O/P=N integral ratio to 1:35 (Spectrum VI in Fig. 2A). Additional experiments confirmed the importance of combining dark and inert atmospheres to minimize phosphine oxidation during the Staudinger reaction. Indeed, the –$ArPh_2P$=O/P=N integral ratio increased to 1:25 and 1:20 for dark/air and light/argon combination, respectively (Fig. 2A, spectra V and IV). It should be noted that the photocatalytic oxidation of Ph_3P to Ph_3P=O is well known in the literature and has been shown several times to occur through a Ph_3P radical cation (Ph_3P^{+}), formed in a photoinduced single-electron transfer (SET) reaction with the photocatalyst and subsequently reacting very rapidly with water or oxygen[36–38]. Based on the literature and our four control experiments, we arrived at the following hypothesis (Fig. 2B). The oxidation of phosphines (Ph_3P–Ar–) to phosphine oxides (–$ArPh_2P$=O) is catalyzed by PAIP itself immediately after its formation in the reaction mixture. Namely, when the Staudinger reaction is carried out under the conditions of visible light and air, the resulting PAIPs act as a "photocatalyst" and generate reactive oxygen species (ROS), which are responsible for the formation of –$ArPh_2P$=O via the photoinduced SET reactions mechanism. The problem with –$ArPh_2P$=O end-groups is that phosphorus loses its nucleophilicity, rendering initial bis-phosphine monomers and later the chain-ends in nascent PAIPs non-reactive. Finally, to find out which ROS are formed during the Staudinger reaction, two more control experiments were carried out. For this purpose, 1,4-hydroquinone (HQ, $O_2^{\cdot-}$ quencher) and triethylenediamine (DABCO, $^1O_2$ quencher) were added to the reaction mixture. According to the ^{31}P NMR analysis, HQ inhibits the photocatalytic oxidation of R_3P better (integral ratio of 1:6) than the presence of DABCO (integral ratio of 1:2.5), resulting in 57% or 14% fewer R_3P=O groups formed in the presence of HQ or DABCO, respectively, compared with the initial reaction conditions (Spectra III and II in Fig. 2A). This indicates that $O_2^{\cdot-}$ is the dominant ROS formed during Staudinger reaction and photooxidizes

Ph_3P–Ar–. While PAIPs have been successfully obtained from electron-deficient aryl azides (activated)[30,39], attempts with electron-rich aryl azides (inactivated) have been less successful in the literature, due to significantly lower reaction rates (up to 3 orders of magnitudes)[29,31,40]. We explored the scope of polymerization for monomers with varying electronic and steric properties and demonstrated that both activated and inactivated azides can undergo Staudinger reaction under the optimized conditions established herein.

Scope of the Staudinger reaction

The screening experiments with different substrates are summarized in Fig. 3. Polymerization was carried out by stirring equimolar amounts of multiazide (**2a–e**; Fig. S1) and (refined) bis-phosphine (**3a**, **3b**; Fig. 3) monomers in DMF at room temperature under an argon atmosphere. The reaction of (**3a**) with the unsubstituted and electron-deficient azides, i.e., 1,4-diazidobenzene (**2a**) and 4,7-diazido-2,1,3-benzothiadiazole (**2b**), resulted in quantitative yields (99%, Fig. 3). Both PAIPs **4aa** and **4ba** were prepared as insoluble powders (orange and purple). Moreover, we found out that the substituents in the aryl azide strongly influence the rate of polymerization, with the electron-withdrawing benzothiadizole core being the fastest, i.e., N_2 evolution started in about 5–10 s, and the electron-donating 9,9-dioctyl-fluorene core being the slowest, as nitrogen formation was barley observed, being consistent with the kinetics of the Staudinger reaction[41].

Next, 1,3,5-triazidobenzene (**2d**) and 1,3,5-tris(4-azidophenyl)benzene (**2e**) were studied for the Staudinger reaction. A pronounced steric effect on the polymerization rates for monomers with trifunctional azide aromatic core was found. First, 1,4-bis(diphenylphosphino)benzene (**3a**) was reacted with **2d**, and surprisingly, no polymer precipitated. However, the reaction mixture turned green-brown, indicating that the reaction had occurred, but probably to a limited extent, which was later confirmed by in situ ^{31}P NMR experiments. Indeed, monitoring the reaction for 24 h with ^{31}P NMR revealed that only one of the phosphine groups in **3a** reacts with the azide groups in **2d** (Fig. S8A). It is suggested that the proximity of the azide groups in **2d** and the steric size of the pendant phenylene groups on the phosphine in **3a** impede the nucleophilic attack of the second phosphine group and further intramolecular cyclization with the formation of a four-membered ring intermediate structure, which significantly slows the rate of Staudinger reaction and allows photooxidation of the Ph_3P–Ar– groups of the bis-phosphine monomer (Fig. S8B). Moreover, the reaction of **3a** with **2e**, an "extended" version of **2d**, resulted in the **4ea** with high yields (90%, Fig. 3) and excellent conversions (99%), confirming the influence of steric in **2d** on Staudinger reaction. The monomer scope was completed with the synthesis of ferrocene-containing PAIPs by reacting bis(diphenylphosphino)ferrocene (**3b**) with **2a** and **2e**. Because of the poor solubility of **3b** at room temperature, the reaction was carried out at 80 °C in DMF and proceeded very rapidly to give **4ab** (orange precipitate) and **4eb** (orange precipitate) with high yields (88–93%, Fig. 3). The precipitates were insoluble in common organic solvents so that only characterization in the solid-state was possible. At this point, it should be emphasized that this is the first example of a PAIP-type metallopolymer containing a ferrocene unit in the π-conjugated backbone (vide infra).

The observed differences in yields can be explained by theoretical calculations, which were performed using DFT at the wB97X-D/6-311 + *G*(*d*,*p*) level. As already Tian and Wang have shown[42], the Staudinger reaction proceeds both for the unsubstituted reactants and for several substituted variants via a *cis*-intermediate. Evaluating the cis, trans, or the one-step mechanism for the monomers of **2a–e** (see S1) and **3a**, **3b** (possessing only one reactive group per compound), we confirm the favorability of the *cis*-mechanism (note that we substitute octyl groups for methyl groups in **2c** due to computational cost since the groups are not involved in the key bond-forming steps and would introduce unnecessary conformational complexity; Fig. 4A). The barriers for the formation of the *cis*-intermediate are 14–26 kcal mol^{-1}, which is about 20 and 35 kcal mol^{-1} lower than for the formation of the trans-intermediate and the one-step mechanism, respectively. In the *cis*-mechanism, the barriers for the formation of the *cis*-intermediate (R_3P-N=N=N–R) and the second step, in which the intermediate is converted into the final iminophosphorane-linkage releasing a nitrogen molecule, are similar.

In general, the first step has a lower barrier for smaller substrates (**4aa**, **4ba**, **4ca**, **4ab**), while this step is slower for bulkier substrates (**4ea**, **4eb**) due to steric hindrance. In Fig. 4, the reaction energy landscape for the formation of the **4aa** polymer and a relationship between the barrier for the formation of the *cis*-intermediate (TS/*cis*) and the experimental yields are plotted, showing a clear correlation.

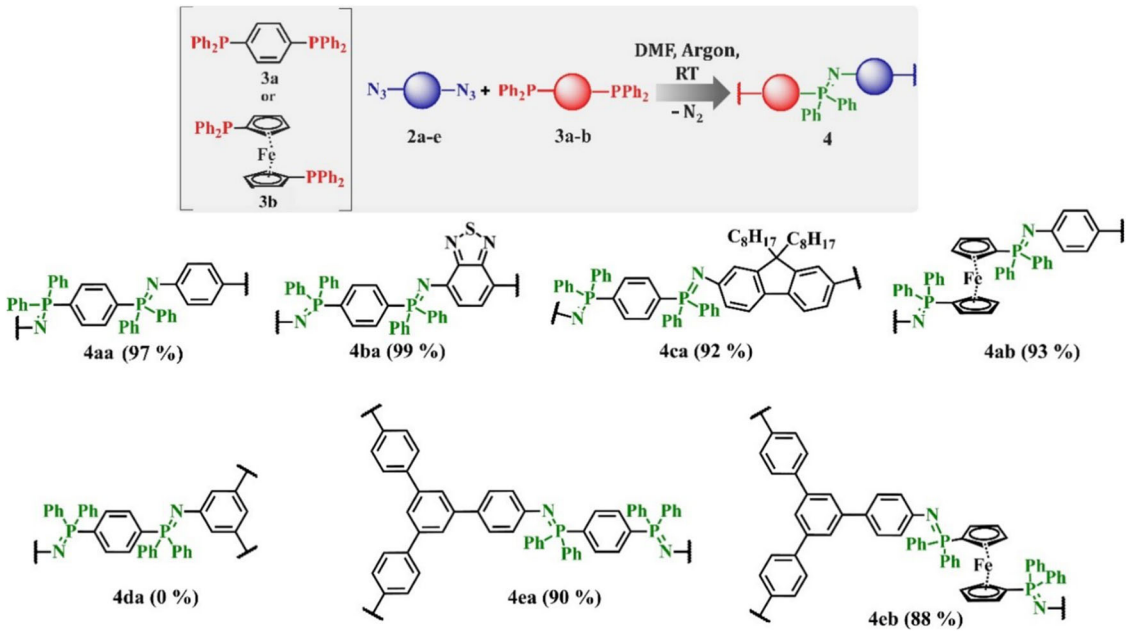

Fig. 3 | Scope of PAIPs with corresponding yields. PAIPs were prepared under ideal conditions determined for polymer **4ca** consisting of DMF as a solvent and under argon atmosphere. The optimised conditions allowed for the incorporation of various electron-donating and withdrawing motifs. Pronounced steric effects were observed in the case of **4da** and **4ea**.

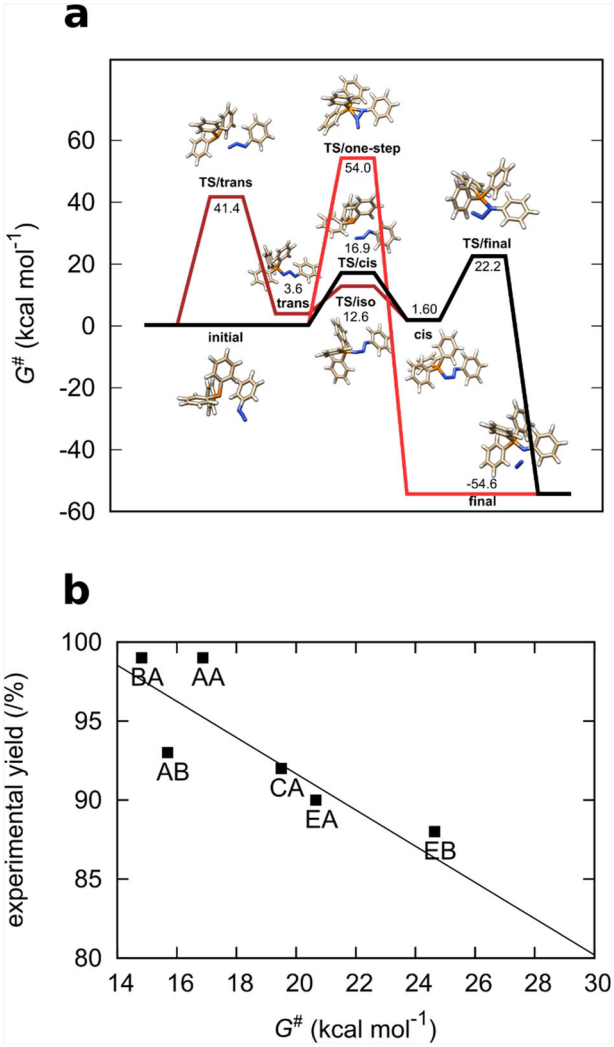

Fig. 4 | Theoretical calculations. Reaction energy landscape for the Staudinger reaction of monomers **2a** and **3a** (**A**), and correlations between the calculated activation barrier and the observed experimental yields for different substrates (**B**), calculated at the wB97X-D/6-311 + *G*(*d*,*p*) level.

Characterization of poly(arylene iminophosphorane)s

Chemical structure. The chemical identity was confirmed by the Fourier transform infrared attenuated total reflection (Fig. S9), solid-state ^{13}C and ^{31}P CP/MAS NMR spectra (Fig. 5A, C), and elemental analysis (SI). As evidenced by FTIR and NMR analyses, all PAIPs consist of corresponding building blocks containing a typical iminophosphorane linkage (–[Ph_2P=NAr]$_n$–). The absence of the characteristic azide absorption band at ~2090 cm^{-1} and the presence of the absorption bands assigned to the P=N vibration at ~1110, 1238, and 1322 cm^{-1} in all the IR spectra (Fig. S9) of the polymers confirm the successful Staudinger reaction[43,44]. Additional absorption bands at ~1436 and ~1500 cm^{-1} were assigned to the C–P vibrations and are found in all FTIR spectra of the polymers and phosphine monomers, respectively[45,46]. The symmetric and asymmetric C–C stretching vibrations of the phenyl rings cause the absorption band at ~1600 cm^{-1}.

Further absorption bands were observed in the case of **4ba**, **4ca**, and **4ab**. In the case of **4ba**, the absorption bands at 1479 and 878 cm^{-1} can be attributed to the C=N and C–S vibrations[47] typical of the benzothiadiazole core, in the case of **4ca**, the absorption bands at 2930 and 2840 cm^{-1} correspond to the C–H vibrations of the methyl and methylene groups of the 9,9-dioctylfluorene core and in the case of **4ab**, the absorption band at 1189 cm^{-1} belongs to the ferrocene unit[48]. The ^{13}C CP/MAS NMR spectra (Fig. 5A) show the most intense peaks at chemical shifts (δ) of 126 and 130 ppm in all polymers corresponding to phenyl carbons ($\underline{C}_{Ar}$–H), while the aromatic carbons in close proximity to the phopsphazene linkage ($\underline{C}_{Ar}$–N=PR_3) appeared at ~150 ppm, and at ~117 ppm in case of **4ba**. The incorporation of the benzothiadiazole and the 9,9-dioctylfluorene core into the PAIPs structure is further confirmed by the characteristic peaks at 154 ppm ($\underline{C}_{Ar}$=N) for **4ba** and the signal at 117 ppm (*m*-$\underline{C}R_2H$) in **4ca**. In addition, more peaks were observed in **4ca** between 40 and 12 ppm belonging to the methylene (–$\underline{C}H_2$) and methyl (–$\underline{C}H_3$) groups of the aliphatic side chains, while the peak at 53 ppm belongs to the tertiary carbon (C–C) in the cyclopentadiene structural unit associated with the alkyl chains. For polymers **4ab** and **4eb**, a new peak appears at 72 ppm belonging to carbons in the cyclopentadiene unit of ferrocene. The ^{31}P CP/MAS NMR spectra (Fig. 5C) show a very broad peak for the phosphorus in the iminophosphorane linkage at ~−3 ppm for all samples, while the peak at ~27 ppm, which corresponds to the –ArPh_2P=O polymer chain ends, is significantly reduced compared to the polymers synthesized in air (Fig. S4). Moreover, there is no peak for the unreacted phosphine monomer at −6 ppm, which is further evidence of complete monomer conversion.

Thermal and thermal/oxidative stability. Thermal properties such as thermal stability and oxidative decomposition behavior of the PAIPs were investigated by TGA and DSC measurements. The corresponding data are listed in Table S1, and the curves are shown in Figs. 5B and D, S10, and S11. The TGA analysis revealed that produced PAIPs have extremely high thermal stability and remain intact up to 350 °C in both the N_2 and air streams. In particular, both $T_{0.1}$ and T_{max} were found to vary between 356–407 and 360–514 °C respectively, in N_2 (Fig. 5B) and 395–475 and 443–548 °C, respectively, in air atmosphere (Fig. S10). The high thermal stability also prompted us to carry out an isothermal TGA. The **4ea** was tested and compared with poly(arylene cyano-vinylene)[49] and poly(imine)[50], conjugated polymers recently prepared in our group. The isothermal step was maintained for 60 min in an air flow after reaching the target temperature, i.e. 400 °C. As can be seen from the isothermal thermograms (Fig. 5D), the mass of the PAIP decreases by 8% in the first 20 min, probably related to the desorption of solvents and moisture, and then remains stable for a further 60 min. The masses of poly(imine) and poly(arylene-cyano-vinylene) on the other hand, decrease by 20% and 25%, respectively, in the first 20 min and then just continue isothermal degradation, losing 25% and 40% of mass within the next 60 min. The isothermal TGA thus confirms the impressive thermal stability of PAIPs, which is due to the presence of thermally very stable phosphorus (λ5, σ4) in the –[Ph_2P=NAr]$_n$– linkage.

Optoelectronic properties. The optoelectronic properties of the PAIPs were further investigated using UV–Vis–DR spectroscopy where the absorption maxima and the corresponding absorption edges were determined and confirmed by the theoretical calculations. The absorption maxima were found at 265, 268, 440, 305, 359, and 412 nm and corresponding absorption edges were positioned at 607, 743, 615, 533 632, and 627 nm for **4aa**, **4ba**, **4ca**, **4ea**, **4ab**, and **4eb**, respectively (Fig. S12). The estimated E_g^{opt} values derived from Kubelka–Munk plots were found 2.11, 1.70, 2.07, 2.40, 2.05, and 1.99 eV for **4aa**, **4ba**, **4ca**, **4ea**, **4ab**, and **4eb**, respectively. These results show that all PAIPs are visible-light active materials. To gain insight into the visible-light active properties of these polymers, the absorption maxima were further investigated by TD-DFT calculations, starting for the dimers of **4aa**, **4ba**, **4ca**, **4ea**, **4ab**, and **4eb**, and found at 230, 246, 291, 276, 264, and 278 nm, respectively. As expected, these values calculated for dimers are consistently lower than the experimental data recorded for the polymers having longer conjugated chains. Moreover, the peaks and entire spectra shift bathochromatically when increasing the number of monomer units in the polymer chain in the TD-DFT calculations (Fig. 6A), with an almost linear dependence of absorbance maxima on the number of monomer units (Fig. 6B). The calculations further reveal that the position of the peaks shifts bathochromatically by about 18–20 nm per added monomer

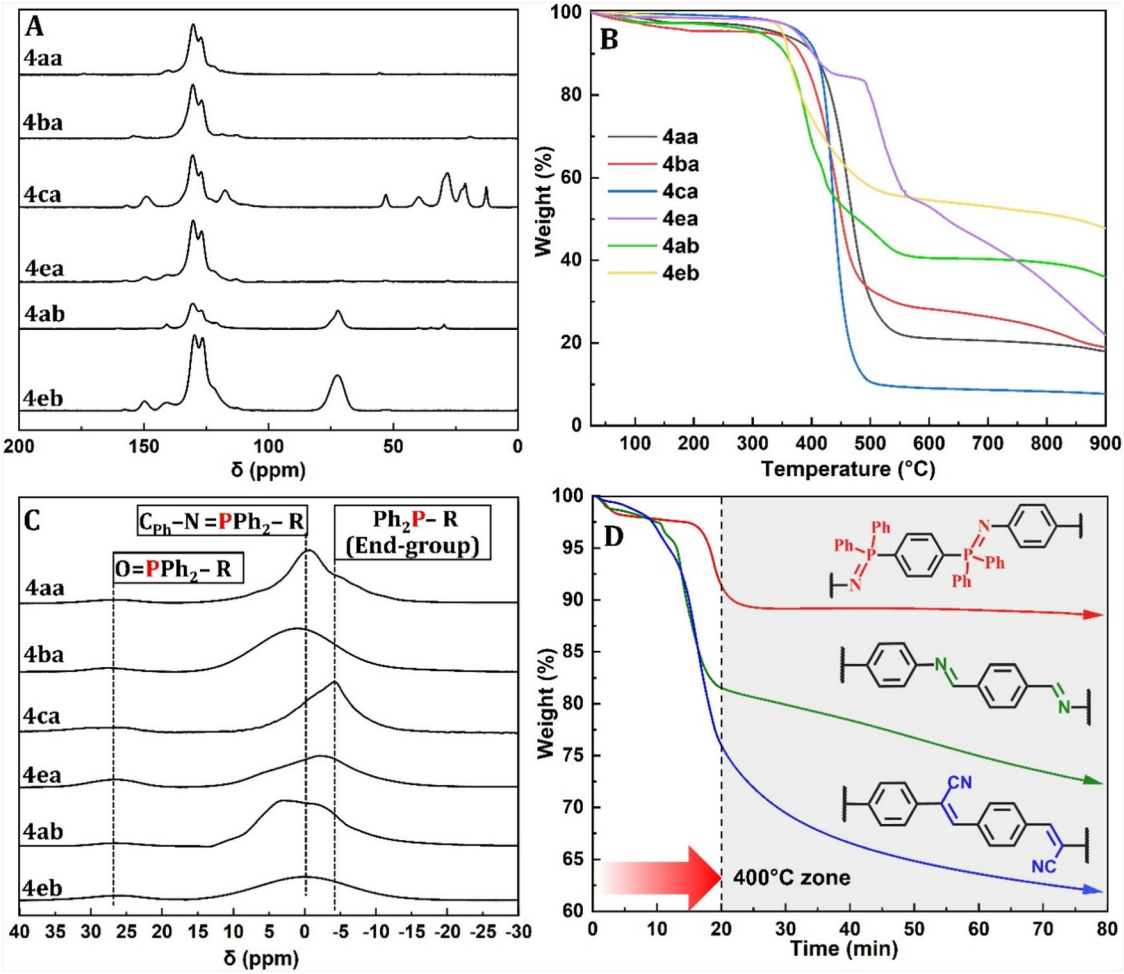

Fig. 5 | Chemical and thermal characterization of PAIPs. ^{13}C CP/MAS NMR spectra (**A**), dynamic TGA under N_2 (**B**), ^{31}P CP/MAS NMR spectra (**C**), and isothermal TGA under air stream (**D**).

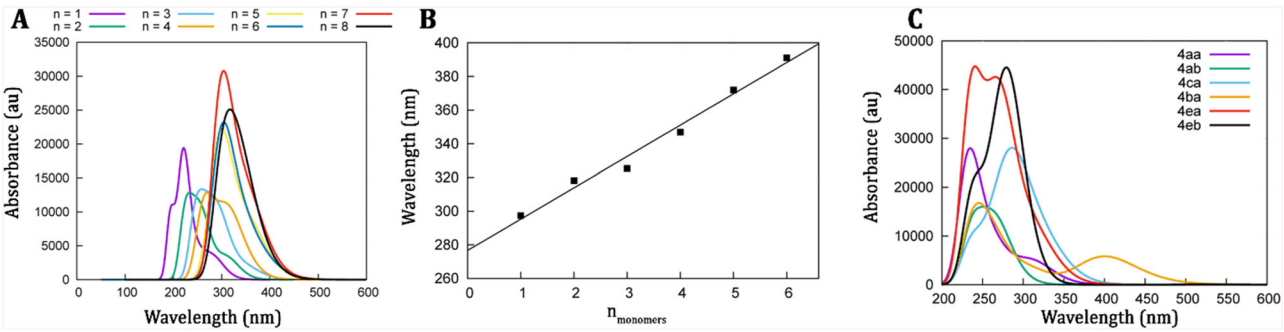

Fig. 6 | TD-DFT calculations. Calculated UV–Vis spectra for oligomers of **4aa** with varied lengths (**A**), the relationship between the lowest-energy (highest wavelength) transition in **4aa** and the number of monomeric units (**B**), and UV–vis spectra for different substrates as dimers (**C**).

unit, suggesting that our PAIPs contain at least 15–20 conjugated repeating monomer units prior to annealing. A distinct secondary peak at higher wavelengths for **4ba** (Fig. 6C), observed both experimentally and computationally, is due to the excitations of the thiadiazole ring. The energetically lower (first) excitations determine the absorption peak at the highest wavelength and, thus the absorption edge. The electronic transition density depicted in Fig. 7, using the natural transition orbital pair (NTO) representation[51], shows the first excitation in the dimers of **4aa** and **4ba**. In **4ba**, the excitations in the thiadiazole ring have lower transition energies than in the ylidic form.

When PAIP powders were annealed above the glass transition temperature (T_g) for a certain time, amorphous, glassy PAIP films were also formed (Figs. 8A and S13), which showed a change in the optical absorption band edges. As shown in Fig. S12, the absorption band edges were bathochromatically shifted by 20–140 nm compared to the original PAIP samples, resulting in a further narrowing of E_g^{opt} by about 0.1–0.5 eV. Thus, the E_g^{opt} of the glassy PAIP films were 1.61, 1.59, 1.85, 1.89, 1.78, and 1.57 eV for **4aa**, **4ba**, **4ca**, **4ea**, **4ab**, and **4eb**, respectively. We believe that the reason for these bathochromatic shifts is the morphological rearrangement and the formation of aggregates of conjugate segments within the PAIP network

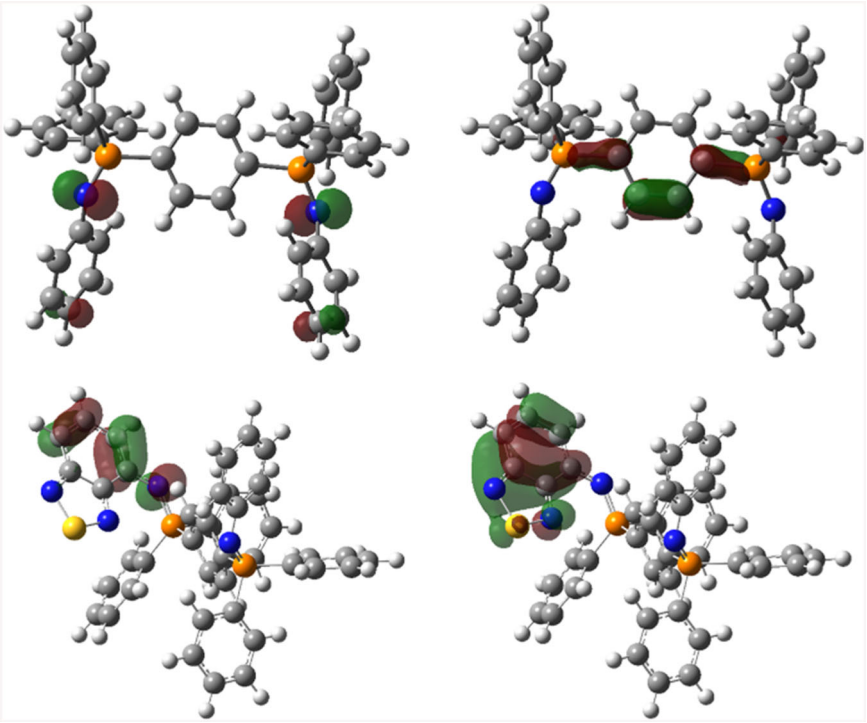

Fig. 7 | Natural transition orbitals. Depiction of the particle (left) and hole (right) with the largest occupations for **4aa** and **4ba** of the lowest (first) excitation.

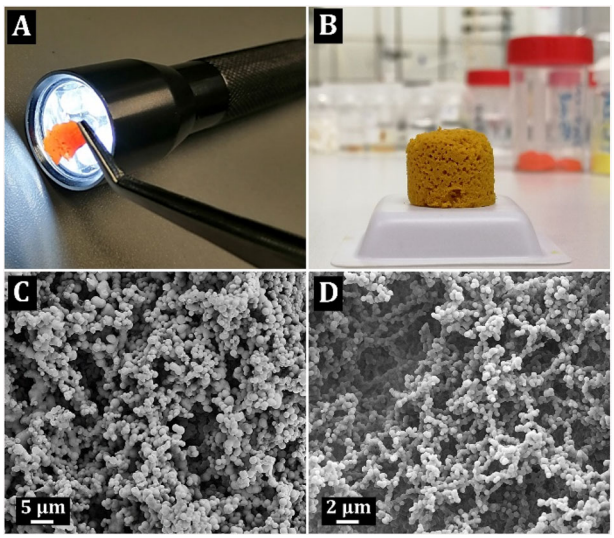

Fig. 8 | PAIP materials. Photo of **4ca** glassy film (**A**), and of **4eb** foam (**B**). SEM image of the foamy structure of **4ea** (**C**) and **4eb** (**D**) poly(arylene iminophosphorane)s.

after thermal annealing, which extends the π-delocalization. Namely, thermal annealing is a common post-synthesis step that allows kinetically trapped (conjugate) segments of the main chains within the polymer network to morphologically rearrange and aggregate[52–54]. In addition, XRD analysis of the PAIPs was performed before and after thermal annealing and revealed no significant changes in the crystallization of the PAIP network (Fig. S14), ruling out the formation of crystalline domains as the cause of the changes in optoelectronic properties. Since an iminophosphorane-linkage can form two resonance structures, i.e., $-[Ph_2P{=}NAr]_n- \leftrightarrow -[Ph_2P^+-{}^-NAr]_n-$[27,55], and the presence of the ylidic form is expected to act as a "conjugation stopper", the visible-light activity of PAIPs was somewhat surprising. Therefore, using the natural bond orbital (NBO) calculations, which is a more intuitive representation than a linear combination of molecular orbitals, we have elucidated the electronic state of iminophosphorane-linkage. The NBO analysis reveals that the natural charges on P, N (and Fe in the ferrocene ring) do not vary significantly among the investigated substrates. In each instance, there is a surplus of electrons on the nitrogen atom ($-1.08e_0$) and a deficiency on the phosphorous atom ($+1.80e_0$). The electron configuration is thus [Ne] $3s^{0.91}$ $3p^{2.19}$ $3d^{0.06}$ for P and [He] $2s^{1.40}$ $2p^{4.66}$ for N. The aromatic rings in ferrocene donate some electron density to the Fe(II) atom, which has a charge of $0.27e_0$ and electron configuration [Ar] $4s^{0.17}$ $3d^{7.47}$. Consistent with a large charge separation in the P–N linkage, NBO calculation suggests a single sigma P–N bond with an occupancy of 1.98 and approximation composition of $0.5638\ P(sp^{2.55}) + 0.8259N(sp^{2.13})$, yielding a 32% localization on P and 68% localization on N. The calculated bond order of the P–N linkage is 0.99 so that the $-[R_2P^+-{}^-NAr]_n-$ resonance structure predominates. However, as already mentioned, the bathochromic shifts of the absorption peaks with an increasing number of repeating units (Fig. 6A) indicate conjugation in the entire system. This can be explained by the presence of a substantial negative-hyperconjugation effect between nitrogen and phosphorus atoms, i.e. an interaction of the lone pair on the nitrogen with the σ^* of the phosphorus, and this has been shown to occur in inorganic iminophosphoranes[27,56,57].

Self-foamed poly(arylene iminophosphorane) monoliths. The preparation of three-dimensional porous monolithic frameworks based on conjugated polymers improves the accessibility of the excited π-conjugated backbone of the resulting materials, which brings additional advantages for various applications[58]. A facile method to achieve porous structural features in π-conjugated polymers is therefore crucial, and we found the Staudinger reaction of particular interest for the preparation of porous poly(arylene iminophosphorane)-based monolithic frameworks. An inherent feature of the Staudinger reaction is the release of nitrogen gas as a by-product. We, therefore, sought to exploit this feature to produce self-foaming PAIP materials in a single step. The synthesis process of PAIP-based foam is described in SI and presented in a video. When an equimolar amount of **2e** and **3a** or **3b** was mixed at room temperature in DMF, the solution immediately turned yellow and nitrogen gas evolved uniformly. However, at this high concentration, the

solubility of the reagents poses a problem, resulting in insufficient release of nitrogen gas required for self-foaming. The same amounts were then mixed in hot DMF (80 °C), where all reagents dissolved and the Staudinger reaction proceeded very rapidly, releasing a large amount of nitrogen gas. Thus, self-foaming and gelation occurred simultaneously, resulting in monoliths with a much greater inflated volume than those at RT (Fig. 8B). Note that no stabilizer is required for the formation of these foams. The porous properties and associated specific surface areas (S_{BET}) were further analyzed by nitrogen adsorption−desorption measurements. The N_2 isothermal data revealed that neither microporosity nor mesoporosity is accessible in either case. Instead, a steep increase in N_2 sorption uptake at $P/P_0 \approx 1$ indicates the presence of macropores (Fig. S15), with S_{BET} of 6 and 7 $m^2\,g^{-1}$ for **4ea** and **4eb**, respectively, which was also confirmed by SEM (Figs. S16 and S17). The SEM analysis revealed a macroporous, foam-like 3D architecture with pores of about 400 µm in diameter (Fig. S16) and pore walls consisting of smaller macropores of about 10 ± 3 µm (Fig. 8C, D).

In summary, a comprehensive study of the Staudinger reaction was carried out and new synthetic conditions for the preparation of poly(arylene iminophosphorane)s (PAIP) were developed. Our systematic photocatalytic experiments have elucidated the roles of visible light and atmospheric oxygen in the oxidation of phosphines (Ph_3P–Ar–) to phosphine oxides (–$ArPh_2P$=O). While other hypotheses remain plausible, our experimental evidence strongly suggests that photooxidation-induced –$ArPh_2P$=O formation is responsible for the slow polymerization rates and the consequent low yields and molecular weights. The introduction of new synthesis conditions employing an inert atmosphere has significantly broadened the scope of PAIPs. This approach allows the synthesis of PAIPs from both electron-deficient and electron-rich organic azides, achieving remarkably high polymerization yields, reaching up to 99%, and expanding the application prospects of the Staudinger reaction. Under these optimized conditions, the Staudinger reaction demonstrates remarkable versatility. The theoretical calculations showed that the different yields of the substrates correlate with the activation barriers. Ground state calculations revealed that the ylidic form, i.e. –$[R_2P^+{}^-NAr]_n$–, is the dominant resonance structure in the iminophosphorane-linkage, while TD-DFT calculations revealed the effects of the different substituents. Given that the predominant resonance structure is the ylidic-form, the activity of PAIP in visible light is somewhat surprising. The latter is probably the result of negative-hyperconjugation, an effect already observed for inorganic iminophosphoranes.

Employing the Staudinger reaction has enabled us to produce unique glassy films, foam structures, and even metallo-polymer hybrids based on poly(arylene iminophosphorane) chemistry. The incorporation of an iminophosphorane linkage into the conjugated backbone is reflected in peculiar optoelectronic properties resulting from the unique electronic structures and high thermal and oxidative stability, even up to 420 °C, compared to conventional conjugated polymers. The isothermal stability is particularly impressive, as the poly(arylene iminophosphorane)s remained completely stable in an air atmosphere at 400 °C for 60 min without losing its semiconducting properties. Finally, nitrogen release associated with the Staudinger reaction was exploited to produce innovative self-foamed conjugated poly(arylene iminophosphorane) materials in a single step, which are of interest for various applications such as heterogeneous catalysis, energy storage, or optoelectronics.

This ingenious protocol will enrich the toolbox of transition metal-free alternatives for the synthesis of π-conjugated polymers (CPs) and offers a particularly compelling aspect due to the absence of bis-organometallic or bis-halide monomers in the Staudinger reaction.

Methods

Multiazide synthesis

To a solution of aryl boronic acid pinacol esters (**1a–e**) in a mixture of methanol and chloroform (1:1), sodium azide (3 eq.), and Cu-catalysts in the form of $Cu(OAc)_2$ or CuI (15–25 mol%) were added. The solution was aerated with compressed air at a flow rate of 150 ml/min for 12–30 h at an elevated temperature (55 °C). After reaction completion, the solvents were evaporated under reduced pressure, and crude products (**2a–e**) were purified with column chromatography or crystallization if necessary. Detailed descriptions of synthetic and work-up procedures can be found in SI under supplementary methods.

PAIP synthesis

To a solution of multiazide (**2a–e**) in DMF, phosphine (**3a**, **3b**) was added under constant stirring. The dry solvent was purged with argon prior to the addition of **3**. Polymerization occurred at room temperature, or at 80 °C when **3b** was used due to solubility issues. After reaction completion, the precipitate was collected, washed with DMF and acetone, and dried under reduced pressure. Detailed descriptions of synthetic procedures can be found in SI.

PAIP glassy film formation

PAIP powder (50 mg) was weighed into a glass vial and heated in an oven to 20 °C above T_g for 10 min. This resulted in the formation of a viscous translucent rubber. The rubber was then naturally cooled to room temperature, which resulted in translucent glassy films.

PAIP foam preparation

To a solution of **3** in DMF (80 °C), which was purged with argon, **2e** was added under constant stirring. The reaction proceeded rapidly, and PAIP foams were formed around the evolving nitrogen. The foams were washed with DMF and acetone and dried under a vacuum. Details about preparation and foam properties can be found in SI[59–64].

Data availability

Supplementary information and Supplementary data are available online or directly from the author in the form of a Word document. A film demonstrating how to make PAIP foams is supplied. The raw data that support the findings of this study are available from the corresponding author upon request.

Received: 26 July 2024; Accepted: 8 November 2024;
Published online: 16 January 2025

References

1. Xu, S., Kim, E. H., Wei, A. & Negishi, E. I. Pd- and Ni-catalyzed cross-coupling reactions in the synthesis of organic electronic materials. *Sci. Technol. Adv. Mater.* **15**, 044201 (2014).
2. Usluer, Ö. et al. Metal residues in semiconducting polymers: impact on the performance of organic electronic devices. *ACS Macro Lett.* **3**, 1134–1138 (2014).
3. Krebs, F. C., Nyberg, R. B. & Jørgensen, M. Influence of residual catalyst on the properties of conjugated polyphenylenevinylene materials: palladium nanoparticles and poor electrical performance. *Chem. Mater.* **16**, 1313–1318 (2004).
4. Sari, E., Yilmaz, G., Koyuncu, S. & Yagci, Y. Photoinduced step-growth polymerization of N-ethylcarbazole. *J. Am. Chem. Soc.* **140**, 12728–12731 (2018).
5. Woods, E. F. et al. Light directs monomer coordination in catalyst-free Grignard photopolymerization. *J. Am. Chem. Soc.* **143**, 18755–18765 (2021).
6. Kayser, L. V. et al. Metal-free, multicomponent synthesis of pyrrole-based π-conjugated polymers from imines, acid chlorides, and alkynes. *J. Am. Chem. Soc.* **138**, 10516–10521 (2016).
7. Giraud, L. et al. Upgrading the chemistry of π-conjugated polymers toward more sustainable materials. *J. Mater. Chem. C* **8**, 9792–9810 (2020).
8. Valle, M., Ximenis, M., Lopez de Pariza, X., Chan, J. M. W. & Sardon, H. Spotting trends in organocatalyzed and other organomediated (de) polymerizations and polymer functionalizations. *Angew. Chem. Int. Ed.* **61**, e2022030 (2022).

9. Wang, Q. et al. Effect of end groups on optoelectronic properties of poly(9,9- dioctylfluorene): a study with hexadecylfluorenes as model polymers. *J. Phys. Chem. C* **116**, 21727–21733 (2012).
10. Kuwabara, J., Yasuda, T., Takase, N. & Kanbara, T. Effects of the terminal structure, purity, and molecular weight of an amorphous conjugated polymer on its photovoltaic characteristics. *ACS Appl. Mater. Interfaces* **8**, 1752–1758 (2016).
11. Miyake, J. & Chujo, Y. The aza-Wittig polymerization: an efficient method for the construction of carbon–nitrogen double bonds-containing polymers. *Macromolecules* **41**, 5671–5673 (2008).
12. Uva, A., Lin, A. & Tran, H. Biobased, degradable, and conjugated poly(azomethine)s. *J. Am. Chem. Soc.* **145**, 3606–3614 (2023).
13. Miyake, J. & Chujo, Y. Aza-wittig polymerization: a simple method for the synthesis of regioregular poly(azomethine)s. *Macromolecules* **41**, 9677–9682 (2008).
14. Thompson, B. C., Kim, Y. G., McCarley, T. D. & Reynolds, J. R. Soluble narrow band gap and blue propylenedioxythiophene-cyanovinylene polymers as multifunctional materials for photovoltaic and electrochromic applications. *J. Am. Chem. Soc.* **128**, 12714–12725 (2006).
15. Cao, C. et al. Cyanovinylene-based copolymers synthesized by tin-free Knoevenagel polycondensation for high efficiency polymer solar cells. *J. Mater. Chem. C* **6**, 8020–8027 (2018).
16. Onwubiko, A. et al. Fused electron deficient semiconducting polymers for air stable electron transport. *Nat. Commun.* **9**, 416 (2018).
17. Lu, Y. et al. Rigid coplanar polymers for stable n-type polymer thermoelectrics. *Angew. Chem. Int. Ed.* **58**, 11390–11394 (2019).
18. Jeon, S., Park, S., Nam, J., Kang, Y. & Kim, J. M. Creating patterned conjugated polymer images using water-compatible reactive inkjet printing. *ACS Appl. Mater. Interfaces* **8**, 1813–1818 (2016).
19. Ciftci, S. et al. Horner–Wadsworth–Emmons dispersion polymerization for the production of monodisperse conjugated polymer particles under ambient conditions. *Polym. Chem.* **9**, 2428–2433 (2018).
20. Pastoetter, D. L. et al. Synthesis of vinylene-linked two-dimensional conjugated polymers via the Horner–Wadsworth–Emmons reaction. *Angew. Chem. Int. Ed.* **59**, 23620–23625 (2020).
21. Smith, R. C. & Protasiewicz, J. D. Conjugated polymers featuring heavier main group element multiple bonds: a diphosphene-PPV. *J. Am. Chem. Soc.* **126**, 2268–2269 (2004).
22. Smith, R. C., Chen, X. & Protasiewicz, J. D. A fluorescent (E)-poly(*p*-phenylenephosphaalkene) prepared by a phospha-Wittig reaction. *Inorg. Chem.* **42**, 5468–5470 (2003).
23. Wright, V. A., Patrick, B. O., Schneider, C. & Gates, D. P. Phosphorus copies of PPV: π-conjugated polymers and molecules composed of alternating phenylene and phosphaalkene moieties. *J. Am. Chem. Soc.* **128**, 8836–8844 (2006).
24. Staudinger, H. & Meyer, J. Über neue organische Phosphorverbindungen III. Phosphinmethylenderivate und phosphinimine. *Helv. Chim. Acta* **2**, 635–646 (1991).
25. Rothemund, S. & Teasdale, I. Preparation of polyphosphazenes: a tutorial review. *Chem. Soc. Rev.* **45**, 5200–5215 (2016).
26. Allcock, H. R. & Morozowich, N. L. Bioerodible polyphosphazenes and their medical potential. *Polym. Chem.* **3**, 578–590 (2012).
27. Escobar, M., Jin, Z. & Lucht, B. L. Electron-donating properties of *p*-phenylene phosphine imides: an electrochemical and spectroscopic investigation. *Org. Lett.* **4**, 2213–2216 (2002).
28. Allcock, H. R. *Chemistry and Applications of Polyphosphazenes* (Wiley-Interscience, 2003).
29. Matyjaszewski, K., Montacue, R., Dauth, J. & Nuyken, O. Synthesis of poly (phenyltrifluoroethoxyphosphazene) by direct reaction of trimethylsilyl azide with bis (2,2,2-trifluoroethyl) phenylphosphonite. *J. Polym. Sci. Part A: Polym. Chem.* **30**, 813–818 (1992).
30. Sundhoro, M., Park, J., Wu, B. & Yan, M. Synthesis of polyphosphazenes by a fast perfluoroaryl azide-mediated Staudinger reaction. *Macromolecules* **51**, 4532–4540 (2018).
31. Pomerantz, M. & Victor, M. W. Synthesis and characterization of a series of alternating copolymers (oligomers) containing organo-X5-phosphazene backbone moieties. *Macromolecules* **22**, 9 (1989).
32. Xie, Y. et al. Tetrafluorination of aromatic azide yields a highly efficient Staudinger reaction: kinetics and biolabeling. *Asian J. Chem.* **13**, 1791–1796 (2018).
33. Brown, H. C., Albright, T. A., Freeman, W. J. & Schweizer, E. E. Nuclear magnetic resonance studies. IV.1 The carbon and phosphorus nuclear magnetic resonance of phosphine oxides and related compounds. *J. Org. Chem.* **40**, 3437–3441 (1975).
34. Abel, E. W. & Mucklejohn, S. A. The chemistry of phosphinimines. *Phosphorus Sulfur Relat. Elem.* **9**, 235–266 (1981).
35. Hanton, S. D. Mass spectrometry of polymers and polymer surfaces. *Chem. Rev.* **101**, 527–569 (2001).
36. Yasui, S. & Tsujimoto, M. Investigation of non-Rehm–Weller kinetics in the electron transfer from trivalent phosphorus compounds to singlet excited sensitizers. *J. Phys. Org. Chem.* **26**, 1090–1097 (2013).
37. Yasui, S., Tojo, S. & Majima, T. Effects of substituents on aryl groups during the reaction of triarylphosphine radical cation and oxygen. *Org. Biomol. Chem.* **4**, 2969–2973 (2006).
38. Bonesi, S. M., Protti, S. & Albini, A. Reactive oxygen species (ROS)-vs. peroxyl-mediated photosensitized oxidation of triphenylphosphine: a comparative study. *J. Org. Chem.* **81**, 11678–11685 (2016).
39. Xie, S., Sundhoro, M., Houk, K. N. & Yan, M. Electrophilic azides for materials synthesis and chemical biology. *Acc. Chem. Res.* **53**, 937–948 (2020).
40. Herring, D. L. The reactions of 1,4-bis (diphenylphosphino)benzene with phenyl azide and 1,4-diazidobenzene. *J. Org. Chem.* **26**, 3998–3999 (1961).
41. Leffler, J. E. & Temple, R. D. Staudinger reaction between triarylphosphines and azides mechanism. *J. Am. Chem. Soc.* **89**, 5235–5246 (1967).
42. Tian, W. Q. & Wang, Y. A. Mechanisms of Staudinger reactions within density functional theory. *J. Org. Chem.* **69**, 4299–4308 (2004).
43. Frik, M. et al. In vitro and in vivo evaluation of water-soluble iminophosphorane ruthenium(II) compounds. A potential chemotherapeutic agent for triple negative breast cancer. *J. Med. Chem.* **57**, 9995–10012 (2014).
44. Imhoff, P., Nefkens, S. C. A., Elsevier, C. J., Goubitz, K. & Stam, C. H. Stabilization of Rhodium(I)-and Iridium(I)-alkyl bonds by intramolecular coordination of an iminophosphorane. X-ray crystal structure of [Rh(CH_2PPh_2=N–C_6H_4–CH_3-4) (COD)]. *Organometallics* **10**, 1421–1431 (1991).
45. Liu, Y. L., Liu, Y. L., Jeng, R. J. & Chiu, Y. S. Triphenylphosphine oxide-based bismaleimide and poly(bismaleimide): synthesis, characterization, and properties. *J. Polym. Sci. Part A: Polym. Chem.* **39**, 1716–1725 (2001).
46. Thomas, L. C. & Chittenden, R. A. Characteristic infra-red absorption frequencies of organophosphorus compounds—V: phosphorus—carbon bonds. *Spectrochim. Acta* **21**, 1905–1914 (1965).
47. Rao, C. N. & Kasturi, T. R. Contribution to the infrared spectra of organosulphur compounds. *Can. J. Chem.* **42**, 36–42 (1964).
48. Winter, W. K., Curnutte, B. & Whitcombs, S. E. The infrared spectrum and structure of crystalline ferrocene. *Spctrochim. Acta* **15**, 1085–1102 (1959).
49. Kotnik, T., Žerjav, G., Pintar, A., Žagar, E. & Kovačič, S. Highly porous poly(arylene cyano-vinylene) beads derived through the Knoevenagel condensation of the oil-in-oil-in-oil double emulsion templates. *ACS Macro Lett.* **10**, 1248–1253 (2021).
50. Kotnik, T., Žerjav, G., Pintar, A., Žagar, E. & Kovačič, S. Azine- and imine-linked conjugated polyHIPEs through Schiff-base condensation reaction. *Polym. Chem.* **13**, 474–478 (2022).
51. Martin, R. L. Natural transition orbitals. *J. Chem. Phys.* **118**, 4775–4777 (2003).

52. Root, S. E., Alkhadra, M. A., Rodriquez, D., Printz, A. D. & Lipomi, D. J. Measuring the glass transition temperature of conjugated polymer films with ultraviolet–visible spectroscopy. *Chem. Mater.* **29**, 2646–2654 (2017).
53. Holliday, S., Donaghey, J. E. & McCulloch, I. Advances in charge carrier mobilities of semiconducting polymers used in organic transistors. *Chem. Mater.* **26**, 647–663 (2014).
54. Schwartz, B. J. Conjugated polymers as molecular materials: how chain conformation and film morphology influence energy transfer and interchain interactions. *Annu. Rev. Phys. Chem.* **54**, 141–172 (2003).
55. Gilheany, D. G. No *d* orbitals but Walsh diagrams and maybe banana bonds: chemical bonding in phosphines, phosphine oxides, and phosphonium ylides. *Chem. Rev.* **94**, 1339–1374 (2002).
56. Chaplin, A. B., Harrison, J. A. & Dyson, P. J. Revisiting the electronic structure of phosphazenes. *Inorg. Chem.* **44**, 8407–8417 (2005).
57. Guidi, V. V., Jin, Z., Busse, D., Euler, W. B. & Lucht, B. L. Bis(phosphine imide)s: easily tunable organic electron donors. *J. Org. Chem.* **70**, 7737–7743 (2005).
58. Monie, F., Vidil, T., Grignard, B., Cramail, H. & Detrembleur, C. Self-foaming polymers: opportunities for the next generation of personal protective equipment. *Mater. Sci. Eng. R* **145**, 100628 (2021).
59. Andjaba, J. M. et al. Catalytic synthesis of conjugated azopolymers from aromatic diazides. *J. Am. Chem. Soc.* **143**, 3975–3982 (2021).
60. Powers, I. G., Andjaba, J. M., Luo, X., Mei, J. & Uyeda, C. Catalytic azoarene synthesis from aryl azides enabled by a dinuclear Ni complex. *J. Am. Chem. Soc.* **140**, 4110–4118 (2018).
61. Bräse, S., Gil, C., Knepper, K. & Zimmermann, V. Organic azides: an exploding diversity of a unique class of compounds. *Angew. Chem. Int. Ed.* **44**, 5188–5240 (2005).
62. Guo, X. Q., Zhou, L. P., Cai, L. X. & Sun, Q. F. Self-assembled bright luminescent lanthanide-organic polyhedra for ratiometric temperature sensing. *Chem. Eur. J.* **24**, 6936–6940 (2018).
63. Jordan, A., Stoy, P. & Sneddon, H. F. Chlorinated solvents: their advantages, disadvantages, and alternatives in organic and medicinal chemistry. *Chem. Rev.* **121**, 1582–1622 (2021).
64. Rothemund, S. & Teasdale, I. Preparation of polyphosphazenes: a tutorial review. *Chem. Soc. Rev.* **45**, 5200–5215 (2016).

Acknowledgements

This work was supported by the Ministry of Education, Science and Sport of the Republic of Slovenia and the Slovenian Research Agency (Grants P2-0150, P2-0152, N2-0340, N1-0303, J2-4424, and I0-0039). T.K. and S.K. would like to thank the World Federation of Scientists for their financial support. The authors would like to thank Uroš Javornik (National Institute of Chemistry) for his kind assistance with NMR spectroscopy. A.D. is a Senior Research Associate and would like to thank the National Fund for Scientific Research (F.R.S.–FNRS) for funding and Dr. R. Riva for skillful assistance. The authors gratefully acknowledge the HPC RIVR consortium and EuroHPC JU for funding this research by providing computing resources for the HPC system Vega at the Institute of Information Science, Maribor, Slovenia.

Author contributions

T.K. designed and performed the experiments. T.K., A.D., J.D.W., M.H., A.P. and S.K. conducted the studies and data analysis. T.K. and S.K. supervised the research. A.P. and S.K. acquired funding. S.K. conceptualized the research. All authors contributed to the writing and editing of the manuscript.

Competing interests

The authors declare no competing interests.

Additional information

Supplementary information The online version contains supplementary material available at https://doi.org/10.1038/s42004-024-01362-5.

Correspondence and requests for materials should be addressed to Sebastijan Kovačič.

Peer review information *Communications Chemistry* thanks the anonymous reviewers for their contribution to the peer review of this work.